ISSN 1063-7788, Physics of Atomic Nuclei, 2023, Vol. 86, No. 5, pp. 827–831. © Pleiades Publishing, Ltd., 2023.

ELEMENTARY PARTICLES AND FIELDS
Experiment

Antineutron Reconstruction and Identification in Electromagnetic Calorimeter

P. Gordeev[1),2)*]
for the ALICE Collaboration

Received March 2, 2023; revised April 30, 2023; accepted April 30, 2023

Abstract—The ALICE experiment at the LHC is designed to explore the hot and dense medium produced in heavy-ion collisions, the so-called quark–gluon plasma (QGP). Antineutron production is a poorly explored domain of high energy physics, although it is interesting in the context of hadrons decaying into antineutrons, the interaction of antineutrons with hadrons, and searching for bound states of antineutrons. We present a method for measuring antineutrons by the electromagnetic calorimeter PHOS of the ALICE experiment. An antineutron can be identified by the cluster shape and the energy deposition in the calorimeter, and its momentum can be reconstructed using the time-of-flight information. The proposed method was verified via the reconstruction of $\bar{\Sigma}^{\pm}$ through decays $\bar{\Sigma}^{+} \to \bar{n}\pi^{+}$ and $\bar{\Sigma}^{-} \to \bar{n}\pi^{-}$ with an antineutron identified in the PHOS.

DOI: 10.1134/S1063778823050174

1. INTRODUCTION

Neutron and antineutron reconstruction is a challenging experimental task and there is up to date no measurement published in heavy-ion collisions physics. Besides spectra and flow of $\bar{n}$ one can measure femtoscopic correlations which will complement and check existing pp and $\bar{p}\bar{p}$ measurements. Reconstruction of $\bar{\Sigma}^{\pm}$-hyperons via their decay into $\bar{n}$ and π^{+} (BR = 99.85%), and $\bar{n}$ and π^{-} (BR = 48.31%) [1], can validate the method of antineutron identification and shed light on the mechanism of hyperon production. Antineutron identification provides the possibility to study the interaction of antineutrons with hadrons, and to search for bound states of antineutrons (di-antineutron, tetra-antineutron) [2, 3]. Also, the study of p-$\bar{\Sigma}^{\pm}$ interactions using femtoscopy is important to understand the nature of hyperon–nucleon interactions [4]. Moreover, a cross-check between different $\bar{\Sigma}^{\pm}$ reconstruction methods will allow to reduce systematic uncertainties and verify the results. Below we discuss the setup of the ALICE experiment, method of antineutron identification, and reconstruction, and validation of this method.

[1)]National Research Centre "Kurchatov Institute", Moscow, Russia.
[2)]National Research Nuclear University "MEPhI", Moscow, Russia.
[*]E-mail: pavel.gordeev@cern.ch

2. ALICE SETUP AND DATASET

The ALICE detector setup is described in detail in [5]. In this study we use information from five detectors: ITS, TPC, PHOS, V0A and V0C [6–9].

The ITS and TPC detectors are used for reconstruction and identification of tracks of charged particles. Particle identification is done by the specific energy loss in TPC. The PHOS electromagnetic calorimeter [8] is located at the bottom of the ALICE setup at the distance of 460 cm from the interaction point. PHOS is designed to detect electromagnetic radiation as well as to measure the spectra of neutral mesons through their photon decays. However, it is also possible to use PHOS to reconstruct and identify antineutrons.

In this analysis, p–Pb collisions at $\sqrt{s_{NN}} = 5.02$ TeV are investigated. For real data, p–Pb collisions of 2016 period with Minimum Bias trigger are studied. Minimum Bias trigger is a signal from V0A & V0C detectors [9]. Total collected events for real data—3.1×10^{8}.

DPMJET [10] generated events processed through AliRoot with simulation of all detectors are used as Monte Carlo data. In the Monte Carlo simulation, the realistic time resolution obtained in real data for photon-like clusters, shown in the Fig. 1*a* [12], is applied. The total number of collected events is 2.7×10^{8}.

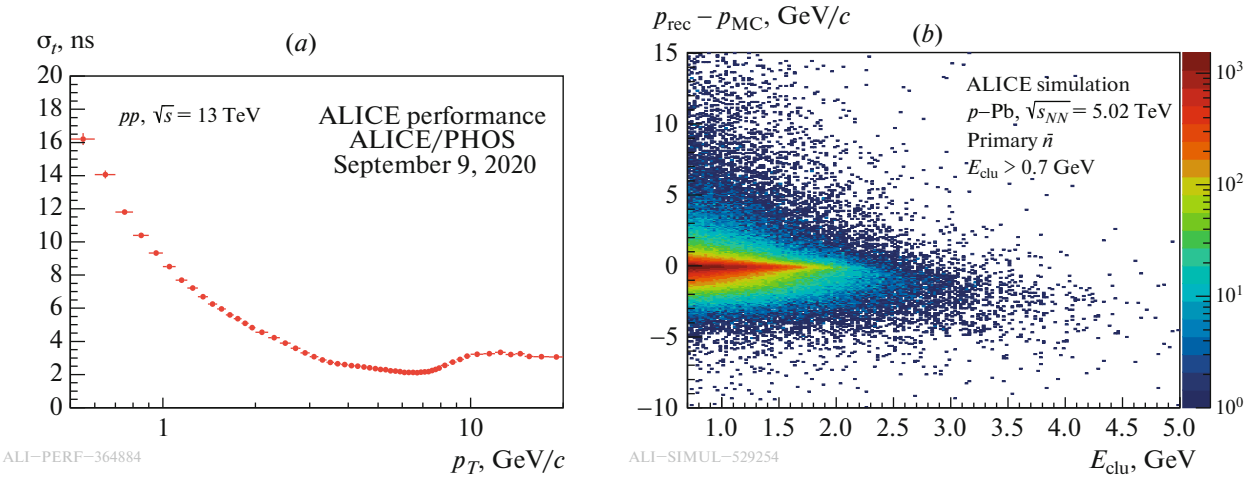

Fig. 1. *(a)* PHOS time resolution obtained for photon-like clusters in *pp* collisions at $\sqrt{s} = 13$ TeV (Adapted from [12], https://doi.org/10.1088/1742-6596/1690/1/012044. By courtesy of CC BY 3.0 licence). *(b)* The difference between reconstructed (p_{rec}) and Monte Carlo (p_{MC}) momentum depending on deposited energy in the calorimeter.

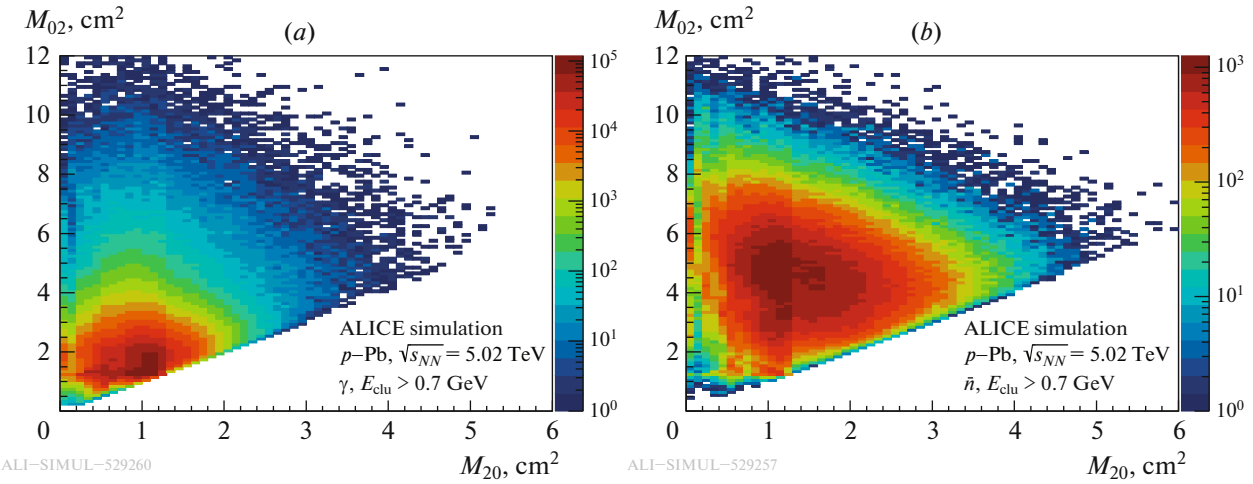

Fig. 2. Distribution of dispersion parameters M_{20} and M_{02} for photon *(a)* and antineutron *(b)* clusters with deposited energy $E_{\text{clu}} > 0.7$.

3. ANTINEUTRON IDENTIFICATION AND RECONSTRUCTION

Antineutrons can be identified in PHOS via 3 criteria: deposited energy, shower shape and neutrality. The annihilation process results in a characteristic energy deposition of about 1.0–1.5 GeV with small dependence on $\bar{n}$ momentum. Second, the shower shape of a cluster (dispersion cut) can be used. Moreover, selection of neutral clusters in a calorimeter using veto of charged particles tracks extrapolated to the calorimeter surface (CPV cut) can be applied in order to increase the purity [11].

A cluster is a set of cells in a calorimeter which has at least a common vertex with another cluster cell [8]. Each cell has two coordinates x an z in the local module coordinate system.

The eigenvalues (M_{20} and M_{02}) of the dispersion covariance matrix can be calculated, and a two-dimensional distribution can be obtained [8]. Fig. 2*a* shows a two-dimensional distribution for photons, and Fig. 2*b*—for antineutrons. For photons, this distribution is more compact and symmetrical than for antineutrons, which allows one to distinguish them from antineutrons.

It is not possible to measure an antineutron momentum via deposited energy due to small dependence on $\bar{n}$ momentum. Therefore, time-of-flight method is used to reconstruct the momentum, which

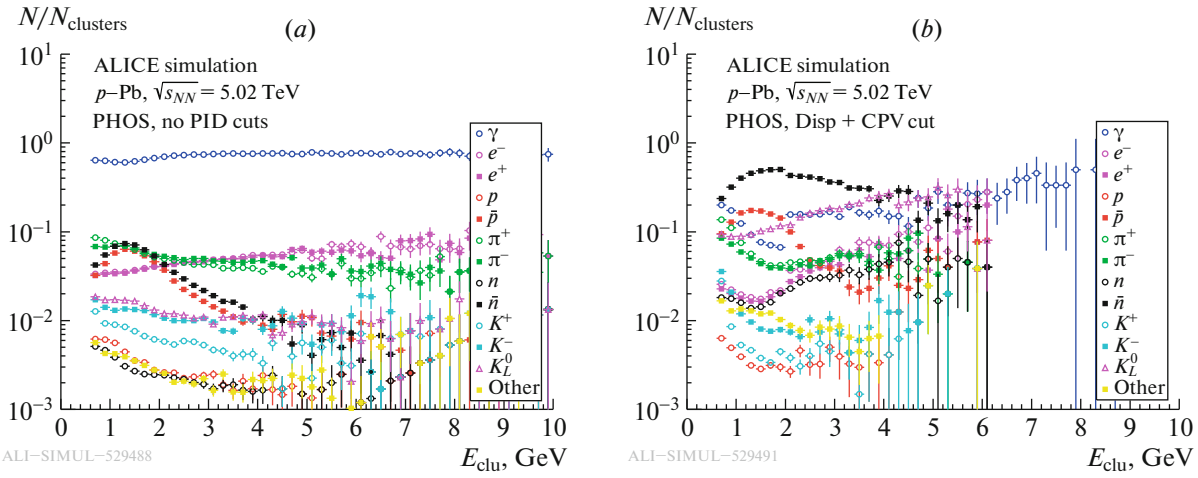

Fig. 3. Fraction of PHOS clusters, produced by different type of particles, without cuts *(a)* and with CPV and dispersion cuts *(b)*.

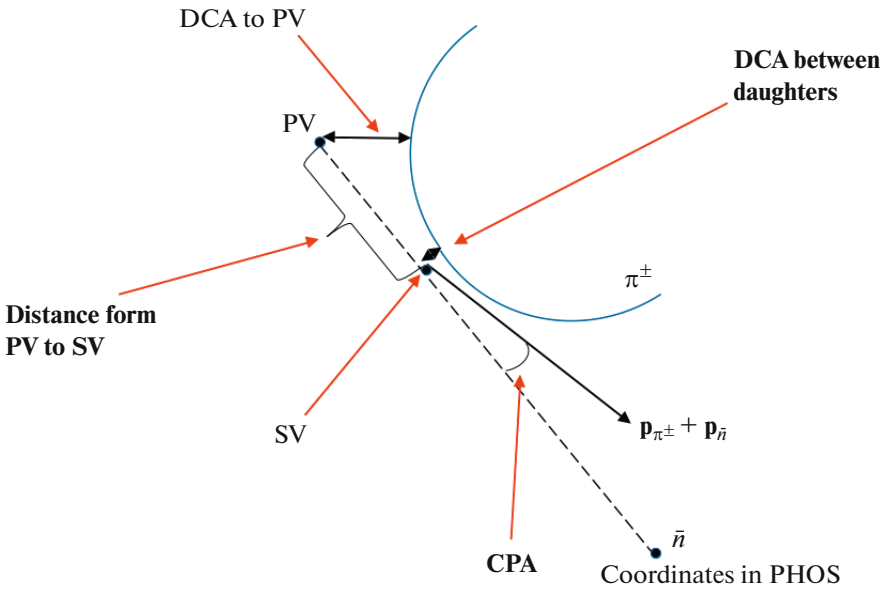

Fig. 4. Scheme of decay topology for $\bar{\Sigma}^\pm$-hyperons. PV—Primary Vertex, SV—Secondary Vertex, CPA—Cosine of Pointing Angle, DCA—Distance of Closest Approach.

is explained below. The absolute value of the antineutron momentum is calculated using the equation:

$$p_{\text{rec}} = \frac{m_{\bar{n}}}{\sqrt{\left(\frac{t_{\text{TOF}} \cdot c}{L}\right)^2 - 1}}, \qquad (1)$$

where L is the distance between primary vertex and cluster coordinate in PHOS; $m_{\bar{n}}$—antineutron mass; t_{TOF}—time-of-flight.

For the momentum direction we assume that $\bar{n}$ passes from the primary vertex to PHOS calorimeter surface. Figure 1*b* shows the difference between the reconstructed and the Monte-Carlo momentum as a dependence of the deposited energy. The asymmetry in this difference leads to asymmetric peaks in the invariant mass distributions for $\bar{\Sigma}^\pm$ hyperons.

4. METHOD VALIDATION

To validate the antineutron identification method, a reconstruction of $\bar{\Sigma}^\pm$-hyperons from their decays to an antineutron and a charged pion was performed. Antineutron reconstruction is provided by PHOS, while charged pion is measured and identified with ALICE central tracking system [6, 7].

The fraction of clusters in PHOS produced by different types of particles before and after the application of CPV and dispersion cut is shown in Fig. 3. The

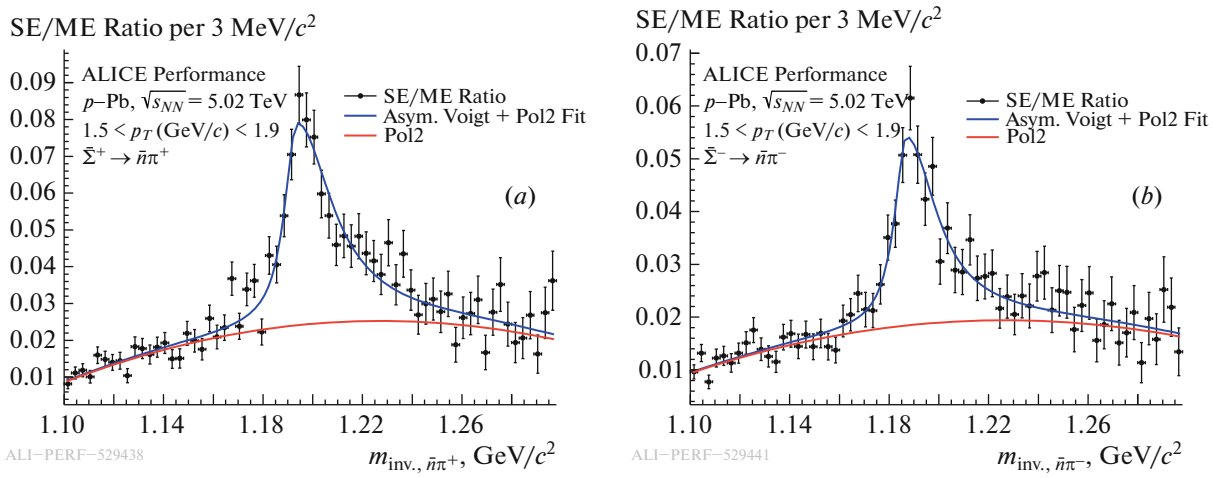

Fig. 5. Same Event to Mixed Event ratio with asymmetric Voigt and second order polynomial fit for $\bar{\Sigma}^+$ *(a)* and $\bar{\Sigma}^-$ *(b)*.

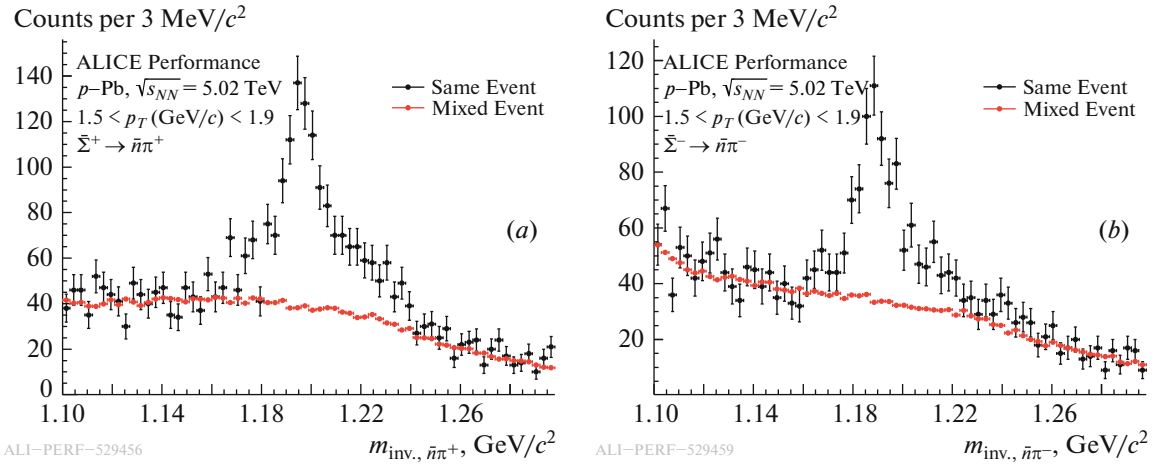

Fig. 6. Same Event and normalized to second order polynomial Mixed Event for $\bar{\Sigma}^+$ *(a)* and $\bar{\Sigma}^-$ *(b)*.

largest fraction before PID cuts belongs to photons, after PID cuts the fraction of antineutron clusters increases to about 50%.

Optional topological selections are developed to increase the signal to background ratio. Several topological parameters can be defined (Fig. 4), but in this study the following are used: the distance of the closest approach between tracks of daughter particles, the distance between primary and secondary vertices, and the cosine of pointing angle, which is the angle between the direction of the sum of daughter momenta and the direction from the primary vertex to the secondary vertex.

After applying all selections, the invariant mass distributions for pairs of a track and a cluster in the calorimeter from one event (Same Event) and from different events (Mixed Event) were constructed. In Fig. 5, the Same Event to Mixed Event ratio is shown for $\bar{\Sigma}^+$ and $\bar{\Sigma}^-$ for $1.5 < p_T^{\Sigma^\pm} < 1.9$ GeV/c. Fitting is done by the sum of the asymmetric Voigt function with independent widths of the left and right sides and the second order polynomial. In Fig. 6, Same Event and Mixed Event normalized to the polynomial is shown. The peak is clearly visible. In Fig. 7, the distribution of the invariant mass of Same Event after subtraction of the normalized Mixed Event is presented. Mean and FWHM values obtained from fitting function are: mean value (1193.9 ± 1.2) MeV/c^2 and FWHM (22 ± 5) MeV/c^2 for $\bar{\Sigma}^+$; mean value (1186.7 ± 1.2) MeV/c^2 and FWHM (19 ± 13) MeV/c^2 for $\bar{\Sigma}^-$. These distributions can be used in the later analysis to obtain the yield of $\bar{\Sigma}^\pm$-hyperons.

5. CONCLUSIONS

For the first time at the LHC, a method of antineutron identification and reconstruction has been

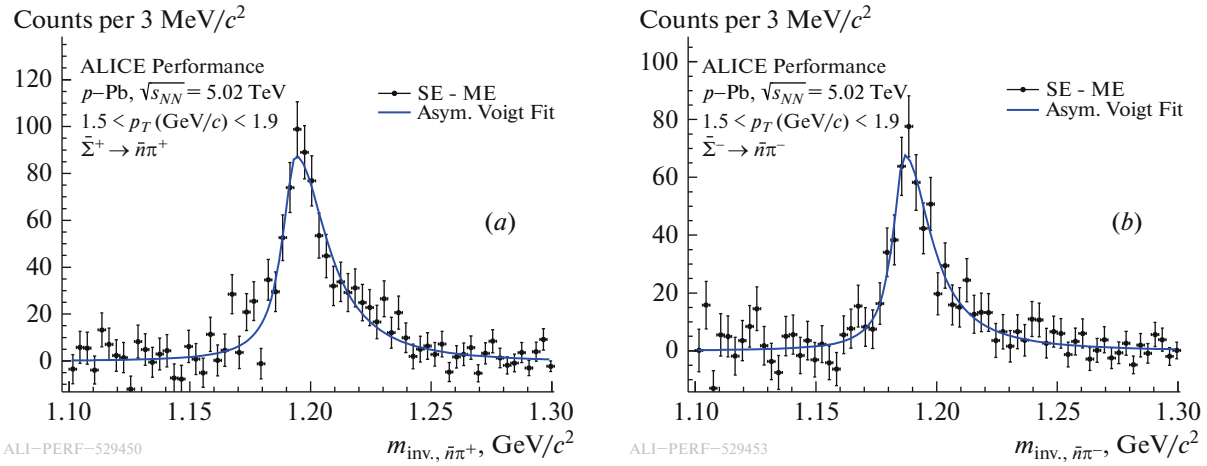

Fig. 7. Same Event after subtraction of normalized Mixed Event for $\bar{\Sigma}^+$ *(a)* and $\bar{\Sigma}^-$ *(b)*.

proposed. The reconstruction of antineutrons by time-of-flight allows to reconstruct their momentum values up to ≈ 2 GeV/c with the available time resolution of PHOS. The method was verified by the reconstruction of the $\bar{\Sigma}^{\pm}$-hyperons via their decays to an antineutron and a charged pion.

FUNDING

We acknowledge support from NRC "Kurchatov Institute" and NRNU "MEPhI".

REFERENCES

1. R. L. Workman et al. (Particle Data Group), Prog. Theor. Exp. Phys. **2022**, 083C01 (2022).
2. M. Duer, T. Aumann, R. Gernhäuser, V. Panin, S. Paschalis, D. M. Rossi, N. L. Achouri, D. Ahn, H. Baba, C. A. Bertulani, M. Böhmer, K. Boretzky, C. Caesar, N. Chiga, A. Corsi, D. Cortina-Gil, et al., Nature (London, U.K.) **606**, 678 (2022).
3. D. Nguyen, C. Neuburger, R. Cruz-Torres, A. Schmidt, D. W. Higinbotham, J. Kahlbow, P. Monaghan, E. Piasetzky, and O. Hen, Phys. Lett. B **831**, 137165 (2022).
4. S. Acharya et al. (ALICE Collab.), Nature (London, U.K.) **588**, 232 (2020); Nature (London, U.K.) **590**, E13 (2021); arXiv: 2005.11495 [nucl-ex].
5. K. Aamodt et al. (ALICE Collab.), J. Instrum. **3**, S08002 (2008).
6. B. Abelev et al. (ALICE Collab.), J. Phys. G **41**, 087002 (2014).
7. C. Lippmann, in *Proceedings of the 2nd International Conference on Technology and Instrumentation in Particle Physics TIPP 2011*; Phys. Proc. **37**, 434 (2012).
8. G. Dellacasa et al. (ALICE Collab.), CERN-LHCC-99-04 (1999).
9. E. Abbas et al. (ALICE Collab.), J. Instrum. **8**, P10016 (2013); arXiv: 1306.3130 [nucl-ex].
10. S. Roesler, R. Engel, and J. Ranft, in *Proceedings of the International Conference on Advanced Monte Carlo for Radiation Physics, Particle Transport Simulation and Applications MC 2000* (2000), p. 1033; hep-ph/0012252.
11. D. Blau (ALICE Collab.), J. Instrum. **15**, C03025 (2020); arXiv: 2001.02928 [hep-ex].
12. D. Blau (ALICE Collab.), J. Phys.: Conf. Ser. **1690**, 012044 (2020).